Velocity derivative skewness in fractal-generated, non-equilibrium grid turbulence

R. J. Hearst and P. Lavoie[a)]
Institute for Aerospace Studies
University of Toronto
4925 Dufferin Street
Toronto, Ontario, Canada, M3H 5T6

The evolution of the velocity derivative skewness, $S(\partial u/\partial x)$, is investigated along two streamwise axes and four transverse positions in the wake of a square-fractal-element grid. In the near-field, the produced turbulence exhibits non-equilibrium characteristics including $C_\epsilon \sim Re_M^\alpha/Re_L^\beta$. In the far-field, the turbulence agrees with canonical grid turbulence results and C_ϵ is approximately constant. It is found that in the non-equilibrium region, the value of $-S(\partial u/\partial x)$ is dependent on both streamwise and transverse position, but after a sufficient decay period, it takes on a near constant value in the far-field. It is demonstrated that the evolution C_ϵ approximately corresponds to that of $-S(\partial u/\partial x)$, which is suggestive that some of the non-equilibrium properties are likely a result of residual strain from the turbulence generating conditions.

The evolution of turbulence in the wake of fractal grids has received considerable attention in recent years. Interest in this area was piqued by the study of Hurst and Vassilicos [1] who identified peculiar features in the turbulence decay behind a series space-filling square fractal grids, including previously unobserved rapid decay of energy and evidence of non-constant normalized dissipation scaling, $C_\epsilon = \langle\epsilon\rangle L/u'^3$, where $\langle\epsilon\rangle$ is the mean dissipation rate of turbulent kinetic energy, L is the integral length scale and u' is the rms of the velocity fluctuations. Turbulence of this type has been termed 'non-equilibrium' turbulence and is summarized in the review by Vassilicos [2]. It has been shown that $C_\epsilon \sim Re_M^\alpha/Re_L^\beta$ with $\alpha \approx \beta \approx 1$ is a robust description of the dissipation in non-equilibrium turbulence[2,3]; $Re_M = U_0 M/\nu$ is the grid Reynolds number based on the mesh length, M, and the velocity immediately upstream of the grid, U_0, and $Re_L = u'L/\nu$ is the local Reynolds number based on the integral length scale and the velocity fluctuations.

Observations of rapid energy decay and non-constant C_ϵ have now also been made in the near-field wakes of regular grids[3], and a square-fractal-element grid[4,5]. However, these studies also showed that the turbulence evolved downstream to a region where C_ϵ was approximately constant. In light of such findings, some researchers[4–8] have suggested that non-equilibrium turbulence does not violate our classical turbulence concepts because it is an artefact of proximity to the grid, and that if measurements are performed a sufficient distance from the grid, many of the classical concepts are recovered; however, this does not negate that non-canonical dynamics and energy cascades may drive the near-field flow[9]. Indeed, different non-equilibrium region measurements have been shown to experience inhomogeneity of the mean flow[4,5,7], turbulent production[5,10,11], transverse transport of turbulent kinetic energy[5,10–12], and non-zero Reynolds stress[5,8,10,11], and it is thus inconclusive which of these mechanisms, if any, are responsible for the non-equilibrium phenomenology. Nonetheless, it is remarkable that one dissipation scaling, $C_\epsilon \sim Re_M^\alpha/Re_L^\beta$, is repeatedly able to approximately collapsed the non-equilibrium dissipation in several experiments, with several different grids, and at several different wake positions.

Recently, Isaza, Salazar, and Warhaft [8] used the velocity derivative skewness,

$$S(\partial u/\partial x) = \frac{\langle(\partial u/\partial x)^3\rangle}{\langle(\partial u/\partial x)^2\rangle^{3/2}}, \tag{1}$$

to facilitate differentiation between the non-equilibrium near-field and the canonical far-field. They reiterated that the canonical Kolmogorov-based phenomenology specifically applies to "systems that are far enough from initial and boundary conditions such that they are not affected by them."[8] This, however, only deals with the asymptotic behaviour of the turbulence and does not address the (perhaps) unexpected findings that non-equilibrium turbulence follows some general scaling laws, nor why such laws should be present in a flow where the boundary and initial generating conditions are still playing an important role. Isaza, Salazar, and Warhaft [8] found that close to a thick-barred regular grid (solidity $\sigma = 0.34$, mesh length $M = 101.6$ mm, and bar thickness $t_0 = 19$ mm) there was rapid decay of energy and constant L/λ (indicative of growing C_ϵ), but in the far-field they observed classical energy decay and $L/\lambda \sim Re_\lambda$ (indicative of constant C_ϵ). They showed that turbulence in the wake of their grid transitioned from a region where $S(\partial u/\partial x)$ was changing to a region where it was constant, and that this corresponded to the

a)Electronic mail: lavoie@utias.utoronto.ca

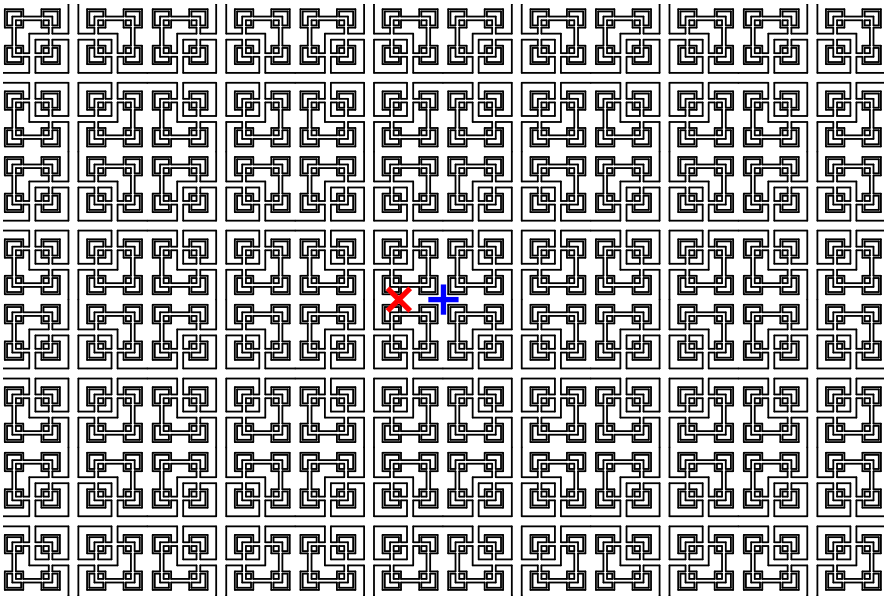

FIG. 1. Schematic of a 60 cm × 40 cm region of the 120 cm × 80 cm square-fractal-element grid. The location of the two streamwise axes investigated here are marked: (+) $(y/M, z/M) = (0.0, 0.0)$, (×) $(y/M, z/M) = (0.3, 0.0)$.

regions that experienced non-equilibrium and canonical grid turbulence phenomenology, respectively. Isaza, Salazar, and Warhaft [8] suggested the changes in $S(\partial u/\partial x)$ were related to residual strain from the turbulence generating mechanisms of the grid, identifying that the flow was not free of its initial generating conditions where $S(\partial u/\partial x)$ was not constant. They then noted that such analysis had not yet been performed in the wake of fractal grids, and it would be required to more rigorously distinguish the near- and far-fields. As such, we present the following analysis to specifically address this concern and link the evolution of $S(\partial u/\partial x)$ to that of C_ϵ.

This letter revisits the data acquired by Hearst and Lavoie [4,5] in the wake of a square-fractal-element grid. Hearst and Lavoie [4] distinguished the near- and far-field by identifying the location where the mean velocity, turbulence intensity, and global isotropy became approximately independent of downstream and transverse position, which occurred at $x/M \approx 20$. Later, Hearst and Lavoie [5] identified the transition between near- and far-field as the location where the scale-by-scale kinetic energy budget for grid turbulence was satisfied, again at $x/M \approx 20$. They further identified that there was non-negligible turbulent production and transverse transport of turbulent kinetic energy for $x/M < 20$. However, no previous fractal study has reported the behaviour of $S(\partial u/\partial x)$, as identified by Isaza, Salazar, and Warhaft [8].

A brief overview of the experiment is provided here before investigating the velocity derivative skewness; for more details, see Hearst and Lavoie [4,5]. The square-fractal-element grid is composed of a series of small, three fractal iteration, square fractals mounted to a 12 × 8 background mesh, as shown in Figure 1. The background mesh has a mesh length of $M = L_0 = 100.0$ mm, and thickness of $t_0 = 6.7$ mm. The lengths of the fractal elements are $L_i = 55.6$, 24.7, and 11.0 mm, where $i = 1, 2, 3$. The thicknesses of the fractal elements are $t_i = 4.1$, 2.5, and 1.5 mm. The solidity of the grid is $\sigma = 0.39$. Here, the downstream distance from the grid is normalized by the mesh length, M, as we have found that this allows for reasonable collapse with other types of grids[4]. However, the 'wake interaction length scale'[13] for the present grid is $x^* = L_0^2/t_0 = M^2/t_0 = 1.49$ m $= 14.9M$, which we provide for reference when comparing to other published fractal works. We also identify that the thickness ratio, the measure of thickest-to-thinnest element in the grid, is $t_r = 4.5$ for the present grid. This is within the lower end of the t_r range tested by Hurst and Vassilicos [1] who showed that increasing t_r improves mean flow homogeneity. Nonetheless, even the $t_r = 17$ grids used in more recent space-filling square fractal studies[11,12] produce turbulence with measurable production within the measurement region, which, by definition, implies there are mean velocity gradients and hence global inhomogeneity.

Data were acquired in the wake of the grid at $Re_M = 65,000$ using constant temperature hot-wire anemometry. In particular, a X-wire was used with a Dantec 56C-series anemometer. The wires of the X-wire were prepared in-house with 2.5 μm tungsten wire with a $\ell = 0.55 \pm 0.05$ mm sensing length. The resolution of the probe ranged $1.4 \leq \ell/\eta \leq 5.6$, where $\eta = \nu^{3/4}/\langle\epsilon\rangle^{1/4}$ is the Kolmogorov microscale. Measurements were performed inside a 1.2 m × 0.8 m × 5.0 m wind tunnel in the range $3.5M \leq x \leq 48.5M$ in $0.35M$ steps along the $y/M = 0.0$ (the

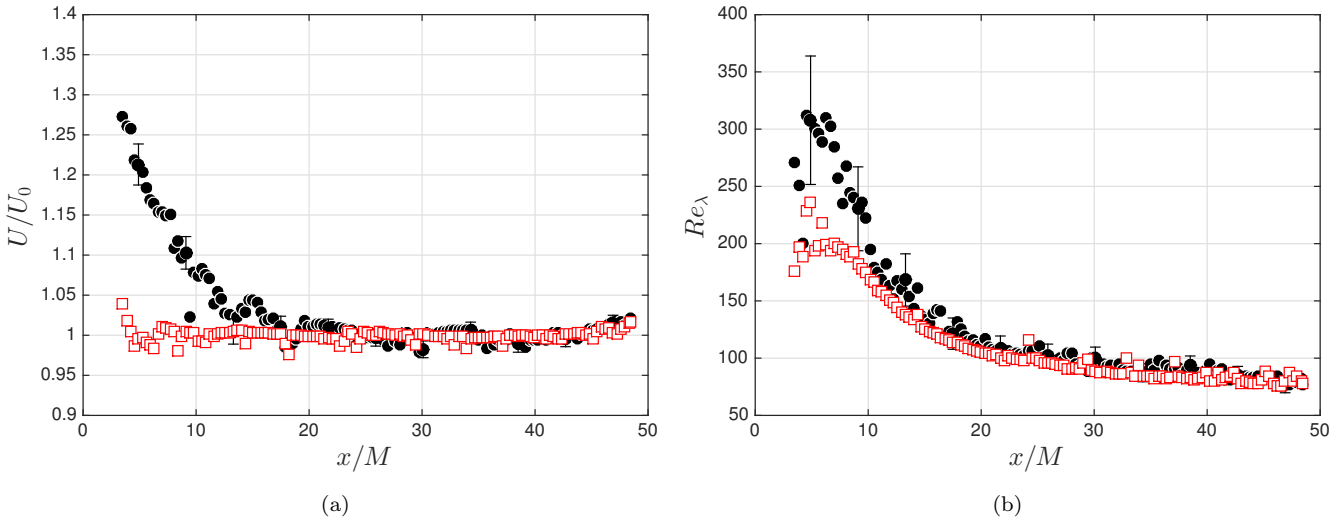

FIG. 2. Streamwise evolution of the (a) normalized mean velocity and (b) local Reynolds number along: (●) $y/M = 0.0$, and (□) $y/M = 0.3$.

centreline of the tunnel) and the $y/M = 0.3$ axes. These axes were chosen to represent cases where $\partial U/\partial x \neq 0$ and $\partial U/\partial x \approx 0$, respectively. The measurement positions are shown relative to the grid geometry in Figure 1 and the evolution of the mean velocity along these axes is shown in Figure 2(a). Transverse measurements were performed between $-2.6 \leq y/M \leq 2.1$ in steps of $0.3M$ at $x/M = 10$, 25, 35, and 45. Measurements were acquired at 30.3 kHz for sufficient time such that samples included a minimum of 10^5 integral time scales. The $\partial/\partial x$ derivatives were calculated assuming Taylor's frozen flow hypothesis, $(\partial \langle\cdot\rangle / \partial t) = U(\partial \langle\cdot\rangle / \partial x)$, which is valid for grid turbulence[14]; the maximum turbulence intensity, $u'/U = 11.5\%$, occurred at $x/M = 4.6$, and it rapidly decayed to 4% by $x/M = 20$ and 2% at the end of the measurement domain. A sixth-order centred-difference scheme was used to numerically compute the gradients, as per the suggestions of Hearst *et al.*[15]. Estimates of the uncertainties are provided as error bars on plots and were calculated for the 95% confidence interval using the bootstrapping technique discussed by Benedict and Gould[16]. For reference, the isotropic estimate of $Re_\lambda = u'\lambda/\nu$ along the two streamwise axes is provided in Figure 2(b) for comparison to previous studies. Note, $100 \leq Re_\lambda \leq 320$ for $x/M < 20$ which is the region that overlaps with previous space-filling square fractals studies[1,11–13]. This is fairly high relative to traditional grid turbulence experiments and does overlap with the Re_λ measured in previous fractal studies.

The velocity derivatives skewness, $S(\partial u/\partial x)$, is shown in Figure 3(a) along the $y/M = 0.0$ and 0.3 streamwise axes, and along the $x/M = 10$, 25, 35, and 45 transverse axes in Figure 3(b). Along the streamwise scans, $S(\partial u/\partial x)$ is collapsed for $x/M \geq 15$. The velocity derivative skewness reaches an approximately constant state for $x/M \geq 20$ at $S(\partial u/\partial x) \approx -0.43$. The reported values of $S(\partial u/\partial x)$ have been corrected for resolution bias using the methodology of Burattini, Lavoie, and Antonia[17] for homogeneous, isotropic turbulence. The streamwise results are verified by the transverse scans, thus identifying that $S(\partial u/\partial x)$ is homogeneous, sufficiently far from the grid. Given the line of discussion presented by Isaza, Salazar, and Warhaft[8], the constancy of $S(\partial u/\partial x)$, as well as the results presented by Hearst and Lavoie[4,5], identify the far-field of the flow induced by the present grid as a classical grid turbulence far-field. The distinction between near- and far-field based on $S(\partial u/\partial x)$ corroborates the distinction between these regions made in our previous work based on transverse homogeneity scans[4] and the scale-by-scale kinetic energy budget[5].

For a Re_λ range that includes the present values, Ayyalasomayajula and Warhaft[18] found that the velocity derivate skewness changed sign and then resettled to its typical far-field value when grid turbulence was subjected to a localized strain. Here, we find that $-S(\partial u/\partial x)$ grows and then becomes approximately settled, suggesting that the strain relationship has a similar evolution[8]. For the present flow, we consider the strain qualitatively with respect to the mean strain rate tensor, $S_{ij} = \frac{1}{2}(\partial U_i/\partial x_j + \partial U_j/\partial x_i)$. Measuring all nine-terms of the strain rate tensor at every location in the flow is difficult and uncommon in experimental investigations, however, we can qualitatively infer where the strain is approximately constant and where it varies through measurements of $\partial U/\partial x$, $\partial U/\partial y$, $\partial V/\partial x$ and $\partial V/\partial y$. Figure 2(a) shows that $\partial U/\partial x \approx 0$ along $y/M = 0.3$, and that it varies before becoming approximately zero along $y/M = 0$ near $x/M = 20$. In both cases $\partial V/\partial x \approx 0$ (not shown here for conciseness). Figure 2 in Hearst and Lavoie[4] shows transverse profiles of U, and that $\partial U/\partial y$ has a spatial dependence for the region $x/M < 20$, and is

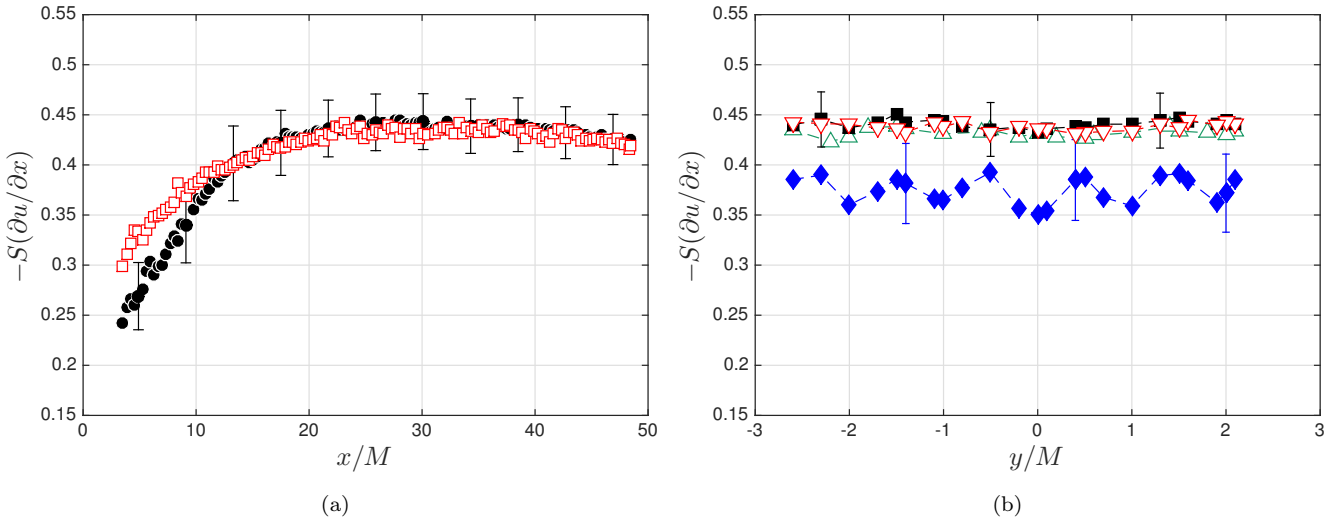

FIG. 3. Measurements of the velocity derivative skewness in the (a) streamwise direction along (●) $y/M = 0.0$, and (□) $y/M = 0.3$, and (b) in transverse planes at (⧫) $x/M = 10$, (▽) $x/M = 25$, (■) $x/M = 35$, and (△) $x/M = 45$

approximately zero thereafter. This can also be inferred from Figure 2(a) of the present study as U along the two axes does not collapse until $x/M \approx 20$. Figure 7(b) of Hearst and Lavoie [5] shows that the same is true of $\partial V/\partial y$. Hence, the region that experiences strain in the present flow corresponds to that with varying $S(\partial u/\partial x)$, as suggested by Ayyalasomayajula and Warhaft [18] and Isaza, Salazar, and Warhaft [8].

As a variation in the strain likely influences the dissipation, we plot the relationship between C_ϵ and $-S(\partial u/\partial x)$ in Figure 4(a). In the far-field, the mean kinetic energy dissipation rate is calculated directly from the turbulent kinetic energy budget for grid turbulence,

$$\langle \epsilon \rangle_{\mathrm{d}} = -\frac{U}{2}\frac{\partial \langle q^2 \rangle}{\partial x}. \tag{2}$$

However, in the near-field, where there is measurable production and transverse transport of turbulent kinetic energy [5], (2) is not an accurate approximation of $\langle \epsilon \rangle$. As such, in the near-field we use the local analogue for the X-wire,

$$\langle \epsilon \rangle_{\mathrm{XW}} = 3\nu \left[\left\langle \left(\frac{\partial u}{\partial x} \right)^2 \right\rangle + 2 \left\langle \left(\frac{\partial v}{\partial x} \right)^2 \right\rangle \right]. \tag{3}$$

This is the same technique used in our earlier work [4,5], and the results are not appreciably different from calculation with the isotropic assumption $\langle \epsilon \rangle_{\mathrm{iso}} = 15\nu \langle (\partial u/\partial x)^2 \rangle$. Measurements in the region $x/M < 7$ in Figure 4(a) are represented by empty symbols, as it is likely that the wakes of the various grid elements are still distinct there [4]. For measurements performed beyond $x/M = 7$, the evolution of C_ϵ and $-S(\partial u/\partial x)$ trend together, and they become approximately constant simultaneously. Moreover, the results from both sets of measurements are collapsed. This would suggest that once the straining of the turbulence by the grid wakes has deteriorated and $S(\partial u/\partial x)$ has reached an approximately constant value, the dissipation has similarly reached a constant state.

For completeness, we also plot C_ϵ against the Reynolds number scaling, Re_M^α / Re_L^β, proposed by Vassilicos and co-workers with $\alpha = \beta = 1$ in Figure 4(b). Note that Re_M/Re_L is proportional to x/M, so this figure also represents the streamwise evolution of C_ϵ. Where C_ϵ is growing, it appears well described by $C_\epsilon \sim Re_M/Re_L$ for both curves. However, the slight curvature in the region $Re_M/Re_L < 200$ is suggestive that $\beta < 1$. Furthermore, rigorously this relationship no longer holds in the far-field as Re_M/Re_L continues to evolve while C_ϵ is approximately constant.

To summarize, based on the findings of Ayyalasomayajula and Warhaft [18] that relate changes in strain to changes in $S(\partial u/\partial x)$, we find that the non-equilibrium region in the present flow coincides with the region where the strain is evolving and has a spatial dependence. When the strain reaches a balanced state, inferred by an approximately constant value of $S(\partial u/\partial x)$ and approximately zero mean velocity gradients in all directions as shown in previous studies with this grid [4,5], then classical grid turbulence conditions are recovered. This result corroborates the findings of Isaza, Salazar, and Warhaft [8] for a different experimental setup, and is the first reporting of $S(\partial u/\partial x)$ in the wake

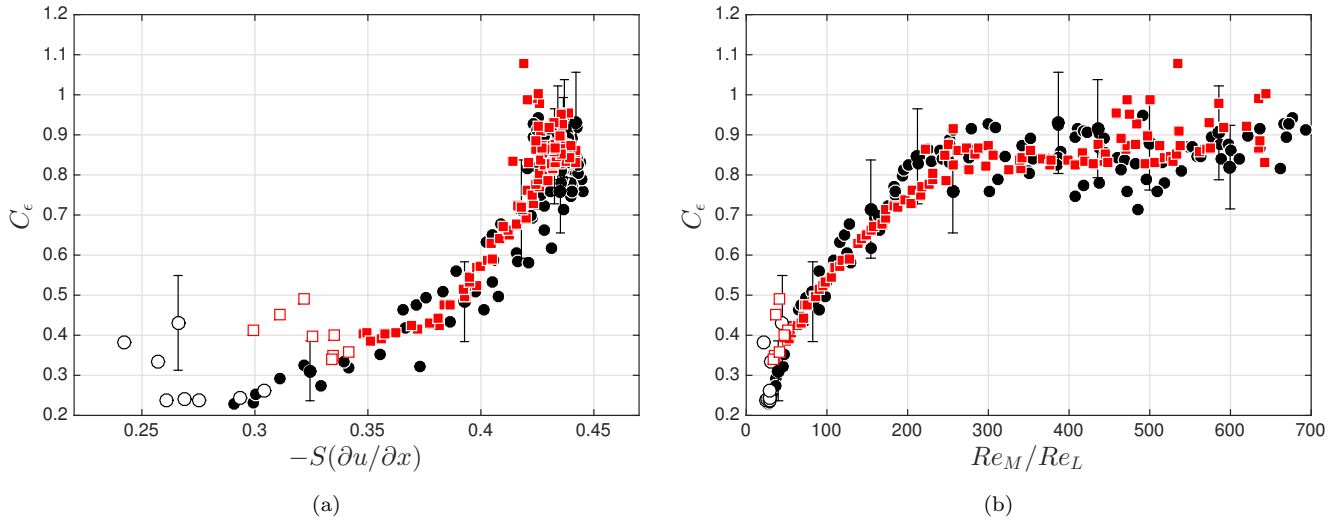

FIG. 4. Variation of the normalized turbulent kinetic energy dissipation rate with the (a) velocity derivative skewness, and the (b) Reynolds number ratio proposed by Vassilicos and co-workers, measured along the streamwise axes (●) $y/M = 0.0$, and (■) $y/M = 0.3$. Empty symbols denote measurements in the region $x/M < 7$.

of a fractal-based generator. It also suggests that the non-equilibrium region is a consequence of residual strain from the turbulence generation, a conclusion promoted by Isaza, Salazar, and Warhaft [8].

Finally, we find here that a relation could be drawn between C_ϵ and $S(\partial u/\partial x)$, which would hold over the whole range of the experiment rather than a subset. While it is difficult to draw any broad conclusions from this observation without a clearer relationship between these turbulence parameters derived from physical arguments, it does show that C_ϵ trends with both small scale ($S(\partial u/\partial x)$) and large scale (Re_L) parameters in the non-equilibrium region. This suggests an interdependence between the small and large scales of the flow. While this may not be surprising for the Re_λ range of the present experiment, it does demonstrate that non-equilibrium properties are present in flows without a significant separation of scales, suggesting that the significance of large scale properties, e.g., mean flow inhomogeneity, cannot be marginalized.

ACKNOWLEDGMENTS

The authors acknowledge the financial support of the Natural Sciences and Engineering Research Council of Canada.

[1] D. Hurst and J. C. Vassilicos, "Scalings and decay of fractal-generated turbulence," Phys. Fluids **19** (2007).
[2] J. C. Vassilicos, "Dissipation in turbulent flows," Annu. Rev. Fluid Mech. **47**, 95–114 (2015).
[3] P. C. Valente and J. C. Vassilicos, "Universal dissipation scaling for nonequilibrium turbulence," Phys. Rev. Lett. **108** (2012).
[4] R. J. Hearst and P. Lavoie, "Decay of turbulence generated by a square-fractal-element grid," J. Fluid Mech. **741**, 567–584 (2014).
[5] R. J. Hearst and P. Lavoie, "Scale-by-scale energy budget in fractal element grid-generated turbulence," J. Turb. **15**, 540–554 (2014).
[6] P.-A. Krogstad and P. A. Davidson, "Freely decaying, homogeneous turbulence generated by multi-scale grids," J. Fluid Mech. **680**, 417–434 (2011).
[7] P.-A. Krogstad and P. A. Davidson, "Near-field investigation of turbulence produced by multi-scale grids," Phys. Fluids **24** (2012).
[8] J. C. Isaza, R. Salazar, and Z. Warhaft, "On grid-generated turbulence in the near- and far field regions," J. Fluid Mech. **753**, 402–426 (2014).
[9] P. C. Valente and J. C. Vassilicos, "The energy cascade in grid-generated non-equilibrium decaying turbulence," Phys. Fluids **27** (2015).
[10] K. Nagata, Y. Sakai, T. Inaba, H. Suzuki, O. Terashima, and H. Suzuki, "Turbulence structure and turbulence kinetic energy transport in multiscale/fractal-generated turbulence," Phys. Fluids **25** (2013).
[11] P. C. Valente and J. C. Vassilicos, "The non-equilibrium region of grid-generated decaying turbulence," J. Fluid Mech. **744**, 5–37 (2014).
[12] P. C. Valente and J. C. Vassilicos, "The decay of turbulence generated by a class of multiscale grids," J. Fluid Mech. **687**, 300–340 (2011).
[13] N. Mazellier and J. C. Vassilicos, "Turbulence without Richardson-Kolmogorov cascade," Phys. Fluids **22** (2010).
[14] S. Corrsin, "Turbulence: experimental methods," in *Handbuch der Physik*, edited by S. Flügge and C. Truesdell (Springer, 1963) pp. 524–589.
[15] R. J. Hearst, O. R. H. Buxton, B. Ganapathisubramani, and P. Lavoie, "Experimental estimation of fluctuating velocity and scalar gradients in turbulence," Exp. Fluids **53**, 925–942 (2012).
[16] L. H. Benedict and R. D. Gould, "Towards better uncertainty estimates for turbulence statistics," Exp. Fluids **22**, 129–136 (1996).

[17]P. Burattini, P. Lavoie, and R. A. Antonia, "Velocity derivative skewness in isotropic turbulence and its measurement with hot wires," Exp. Fluids **45**, 523–535 (2008).
[18]S. Ayyalasomayajula and Z. Warhaft, "Nonlinear interactions in strained axisymmetric high-Reynolds-number turbulence," J. Fluid Mech. **566**, 273–307 (2006).